Supplementary Information (SI) for Dalton Transactions.
This journal is © The Royal Society of Chemistry 2024

Supporting Information

Synthesis of In-Plane Mo_2C/MoO_3 Heterostructures by Novel Spatial-Confined Partial Oxidation Approach for Enhanced TEA Sensing

Liang-Yu Ma[a,1], Zheng-Guang Zhao[a,1], Xuan-Yu Yang[a], Li-Juan Yue[a], Fei-Long Gong[a], Ke-Feng Xie[c], Pan-Pan Zhou[b] and Yong-Hui Zhang[a]**

Characterization:

The crystal structure was measured by powder X-ray diffraction (XRD) analysis on a German Bruker D8 diffractometer system (D8 Advance, Germany) from 5 to 80 ° with Cu Kα radiation (k = 1.54056 Å; 40 Kv, 40 mA; scanning rate 0.1 °/s^{-1}). The thickness of the samples was measured by atomic force microscopy (AFM, Dimension Icon with Nanoscope V controller, Bruker, Germany) in the tapping mode under ambient conditions. The images were processed and analyzed by NanoScope Analysis 3.00 software. The field emission scanning electron microscopy was performed on a JSM-7001F (TEM, JEM-7001F operated at 10 kV, Japan). The microstructure of the catalysts was characterized by transmission electron microscopy (TEM, JEM-2100 operated at 200 kV, Japan). X-ray photoelectron spectroscopy (XPS) spectra was obtained by Thermo Scientific Escalab 250Xi (ESCALAB 250Xi, excitation energy 1486.6 eV, detector resolution 0.45 eV) with monochromatized Al-Kα X-ray as the excitation source. The charge correction was 0.2 eV, which corresponds to the C 1s XPS spectrum (284.8 eV), the Voigt function was the most appropriate function for XPS peak fitting, and Shirley background was analyzed XPS data of samples. Nitrogen adsorption and desorption measurement (Belsorp-mini II, Japan) was characterized to analyze the specific surface area of the samples. Raman spectra analysis was performed on an Acton Spectra Pro500i Raman spectrometer with a 532 nm excitation wavelength and a power of 5 mW (2% of the maximum power). To analyze the molecular structure and chemical composition of samples, FT-IR spectra (Nicolet iS5, Thermo Fisher Scientific, USA) was collected in the range of 400-4000 cm^{-1}. UV-vis-NIR spectra were collected with a Hitachi UV-3600 spectrophotometer in the range of 200-1800 nm. Electron paramagnetic resonance (EPR) measurement was conducted with a Bruker A300 spectrometer. Electrochemical measurements including electrochemical impedance spectrometry, and Mott-Schottky plots were performed on an electrochemical workstation (CHI660D, Chenhua, Shanghai, China) at room temperature. All three measurements were containing Ag/AgCl as the reference electrode, Pt wire as the counter electrode, and the sample on indium tin oxide (ITO, 1 cm^2) as the working electrode. The electrolyte solution contained 0.1 mM of KCl, 5 mM of $K_4Fe(CN)_6{\cdot}3H_2O$, and 5 mM of $K_3Fe(CN)_6$. The Mott-Schottky plots were measured by using 0.1 M Na_2SO_4 solution as the electrolyte. The following steps were

taken to perform an oxygen temperature program desorption (O_2-TPD) analysis: First, 0.2 g of sample was treated in He (20 mL/min) for 1 h at 250 °C and then cooled to 50 °C. Then, O_2 was introduced to be adsorbed on the materials surface and then purged with He (30 mL/min) for 2 h at this temperature to remove the physically adsorbed O_2. The temperature was then raised from 50 °C to 800 °C at a rate of 10 °C/min. The desorption of O_2 was detected by using a thermal conductivity detector (TCD) (Micromeritics, Atlanta, GA, USA). The following steps were taken to perform the hydrogen temperature program desorption (NH_3-TPD) analysis: First, 0.2 g of sample was treated in He (20 mL/min) for 1 h at 250 °C and then cooled to 25 °C. The temperature was then increased from 25 °C to 800 °C at a rate of 10 °C/min in (NH_3/He (2% v/v_0) atmosphere. The consumption of H_2 was detected by thermal conductivity detector (TCD) (Micromeritics, Atlanta, GA, USA).

Fabrication of gas sensor and test method:

Briefly, the as-made samples were firstly ground in a mortar for 0.5 h to form the viscous slurry by dropping in ethanol. The viscous slurry was then coated on an alumina tube (0.5 mm thickness and 4 mm length) with a pair of printed Au electrodes, and dried at 60 °C for 12 h. Finally, a Ni-Cr alloy wire was inserted into the tube as a heater to adjust the working temperature of the gas sensor. To improve stability, all sensors were then aged at 110 °C for 10 days. The WS-30B system (Wei sheng Instruments Co. Zhengzhou, China) was used to investigate the sensor performance. Static volumetric method was used to test the gas sensing. The gas sensor is placed in a sealed 18 L airtight glass test chamber at the beginning. The working temperature of the gas sensor was controlled by adjusting the heating voltage (V heating) of the Ni-Cr alloy resistor. During the test, the analytical reagent solution is injected into the static test system and evaporated with an evaporator. Target gas is injected into the test chamber (liquid sample is injected into the heating plate and evaporated into gas by heating), and a gas mixture with known concentration can be obtained by air dilution. The concentration of target gas was calculated by the following formula:

$$V_x = \frac{v \times c \times M}{22.4 \times d \times p \times 1000} \qquad (1)$$

V_x (μL) is the volume of the liquid, C (ppm) is the concentration of the target gas, ρ (g/mL) is the density of the liquid, d is the purity of the liquid, V (L) is the volume of the glass chamber, and M (g/mol) is the molecular weight of the liquid.

The concentration of the gas can be transferred to the volume of the target reagent and the required test dose can be obtained by microinjector. After injection of the target gas, the test chamber was removed when the sensor resistance reaches the equilibrium value. The analysis system automatically acquires the resistance and response values of the sensor. During the test, a reference resistor (R load) was added to the sensor circuit, operating at 5 V. The response of the sensor in air or target gas can be measured by monitoring the voltage of the reference resistor.

For n-type semiconductor, sensing response is defined as the ratio of resistance in the air (R_a) to the resistance in gas (R_g). The sensing response for reducing gas was calculated using $S = R_a/R_g$ (for oxidizing gas, $S = R_g/R_a$). The response/recovery time

is defined as the time required to reach 90% of the initial equilibrium value.

The donor density was calculated by the slope of Mott-Schottky plots following the below equation:

$$N_d = \left(\frac{2}{e_0 \varepsilon_0 \varepsilon}\right)\left[d\left(\frac{1}{c^2}\right)\Big/ dv\right]^{-1} \quad (2)$$

Where N_d was the donor density, e_0 was the electron charge, ε_0 was the permittivity of vacuum, ε was the dielectric constant of MoO_3 (3)[1] and Mo_2C (4.3)[2], and V was the applied bias at the electrode.

The band gap was calculated by the Tauc equation:

$$(\alpha h\nu)^n = C(h\nu - E_g) \quad (3)$$

Where α was the absorption coefficient, C was a constant, and E_g was the band gap of the semiconductors.

Gas chromatograph-mass spectrometer (GC-MS, Agilent ISQ) was used to analyze the gases produced in the sensing experiment. The GC-MS is equipped with a DB-5MS UI capillary column (30 m × 0.25 mm × 0.25 μm). The experiment was carried out as follows. The GC oven temperature was first held at 40 ℃ for 3 min, then gradually increased to 250 ℃ with a ramping rate of 10 ℃·min-1 to and finally held for 3 min. The 100 μL sample gas was injected into GC at the split ratio of 20:1, and the flow-rate of the He carrier gas is 2 mL·min-1. The quad-rupole temperature is 280 ℃ and the source temperature is 300 ℃. Ionization voltage is 70 eV. The mass spectrometer was acquired in the m/z range of 33 - 500. MS analysis is performed in electron impact (EI) mode. The product composition identification was based on the comparison of MS data using a mass spectral library (NIST08). Typically, the gaseous mixture generated during sensing process was prepared as follows. The as-prepared samples of MCMO-320, MCMO-350, and MoO_3-380 were weighted 10 mg, respectively, and then putted with liquid TEA of 1 μL into the serial headspace bottles. The balance temperature between the sample and TEA was 160 ℃ for 2.5, 5, 10, 20, and 40 min under the condition of sealing and vibrating. For comparison, the mixture of TEA and air in a headspace bottle was balanced at for 5 and 10 min under the same condition.

First-principles calculations based on density functional theory (DFT) were performed in CASTEP package to investigate the in-plane Mo_2C/MoO_3 heterostructures. The ultrasoft pseudopotential was used for electron−ion interactions, and the Perdew−Burke−Ernzerhof (PBE) form of the generalized gradient approximation (GGA) was employed to describe the exchange correlation functional. For the geometry optimization and structural properties, the convergence tolerance of energy is 1.0×10^{-5} Ha, maximum force is 0.002 Ha/Å, and maximum displacement is 0.01 Å.

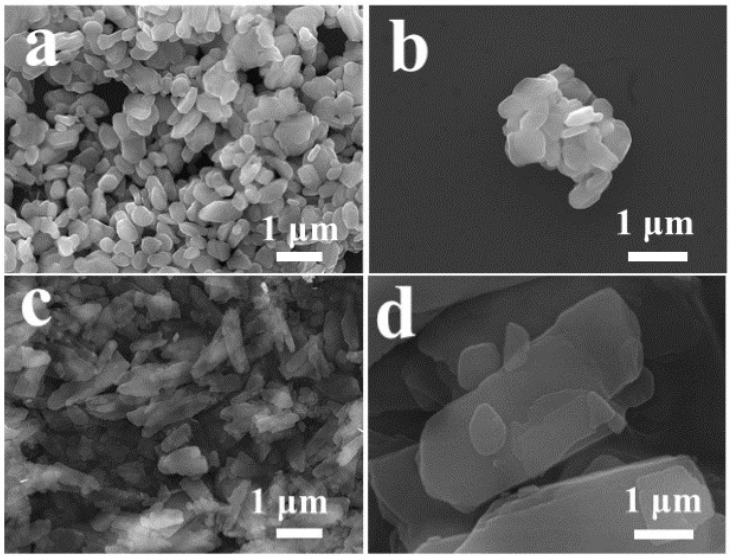

Figure S1. SEM images of (a, b) MoO_3-Bulk and (c, d) MoO_3-DDA.

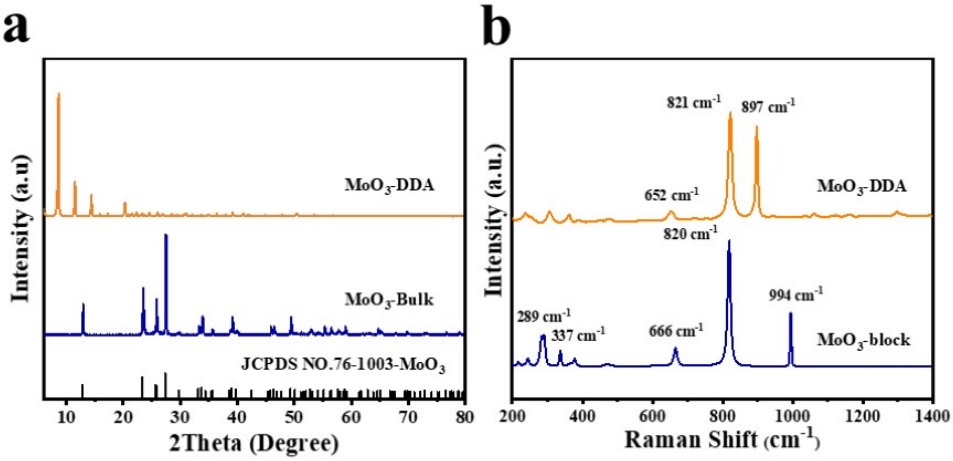

Figure S2. XRD patterns and (b) Raman spectra of MoO_3-Bulk, and MoO_3-DDA.

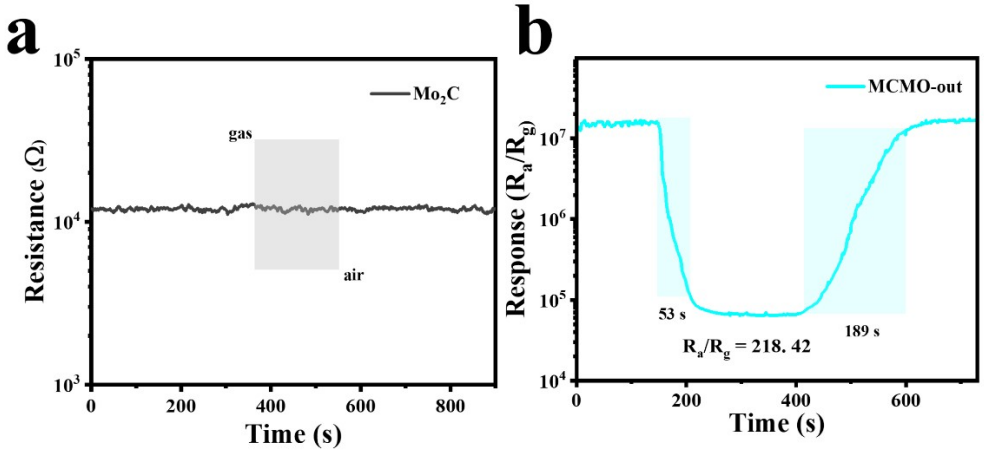

Figure S3. Sensing resistance curve of (a) Mo_2C and (b) MCMO-vertical to 50 ppm TEA at 160 °C.

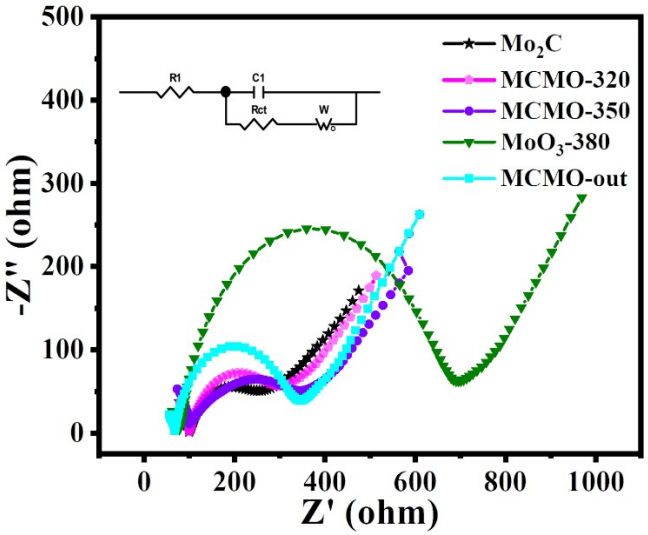

Figure S4. EIS Nyquist plots of Mo_2C, MCMO-320, MCMO-350, MoO_3-380 and MCMO-out.

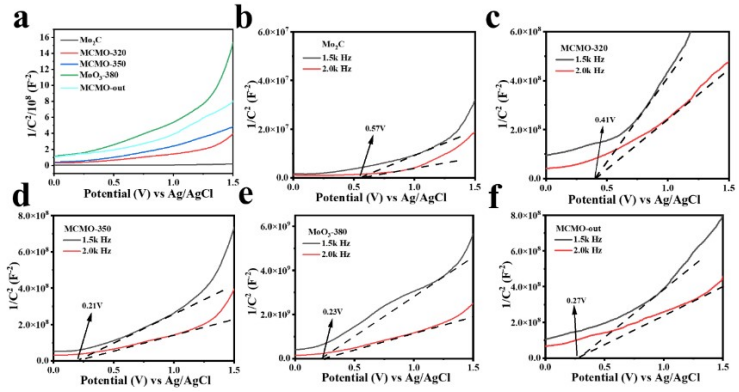

Figure S5. Mott−Schottky plots of (a) all samples (b) Mo_2C, (c) MCMO-320, (d) MCMO-350, (e) MoO_3-380 and (f) MCMO-out.

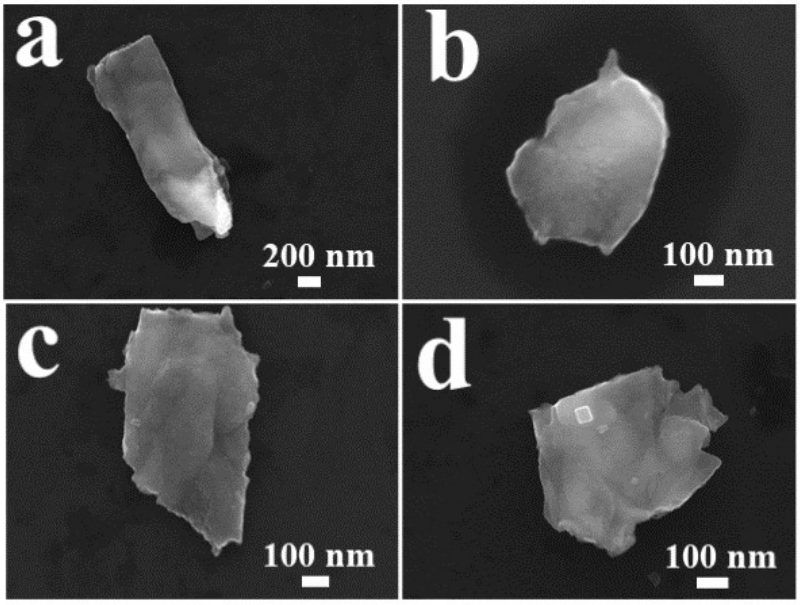

Figure S6. SEM of (a) Mo_2C, (b) MCMO-320, (c) MCMO-350 and (d) MoO_3-380 after testing for 60 days.

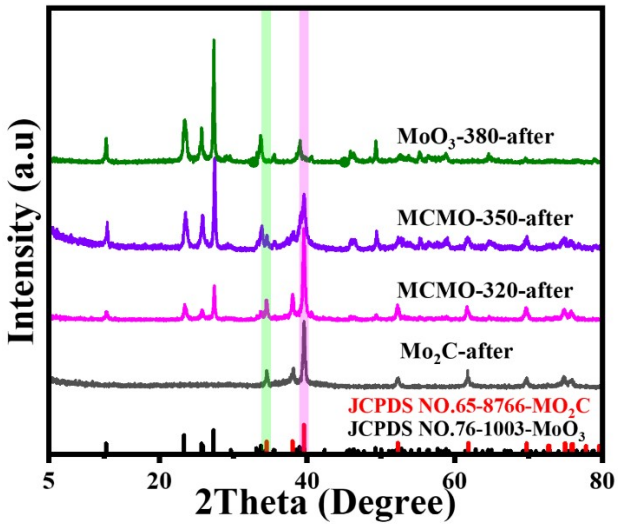

Figure S7. XRD patterns of Mo_2C, MCMO-320, MCMO-350, MoO_3-380 after testing for 60 days.

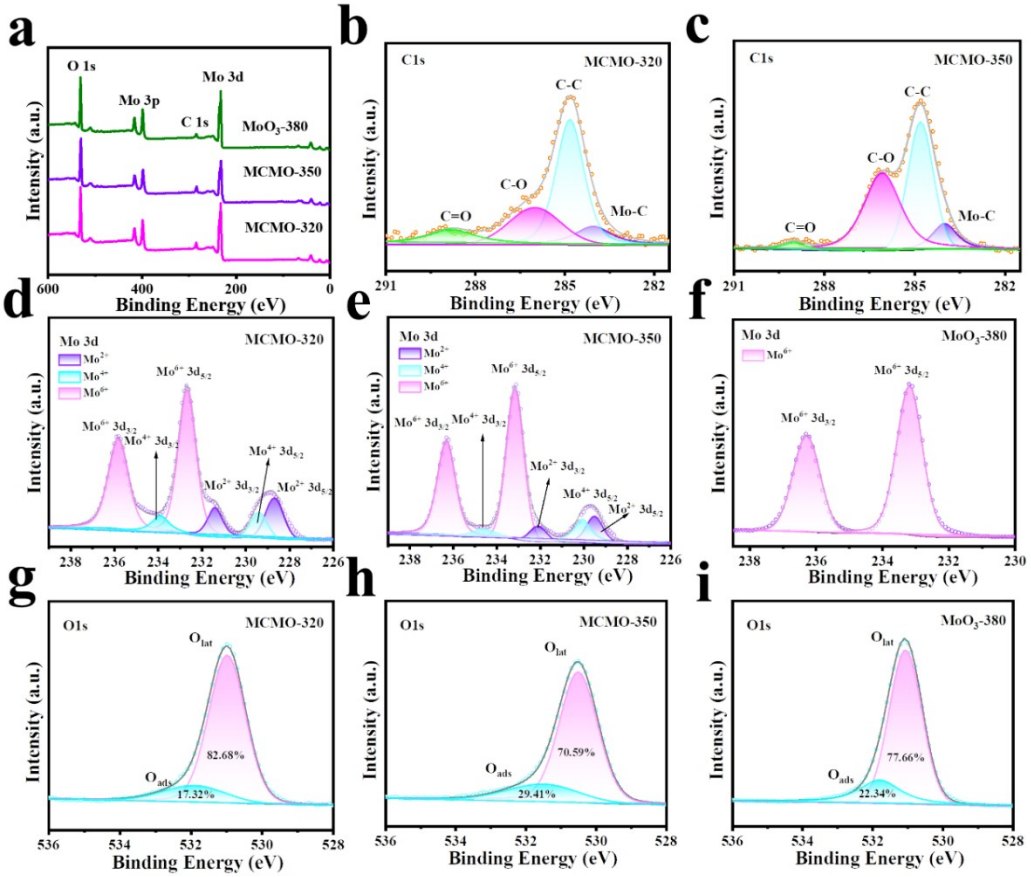

Figure S8. (a) XPS survey spectra of MCMO-320, MCMO-350, and MoO_3-380, C 1s of (b) MCMO-320, (c) MCMO-350, Mo 3d of (d) MCMO-320, (f) MCMO-380, O1s of (g) MCMO-320, (h) MCMO-350, and (i) MoO_3-380 after exposing in TEA.

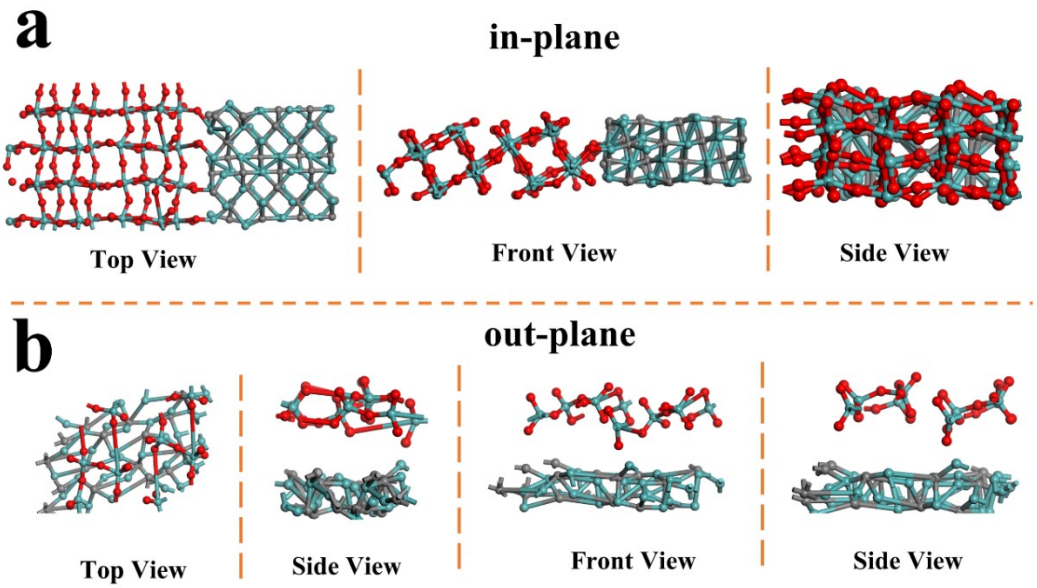

Figure S9. The schematic diagram of well lattice-matched (a) in-plane Mo_2C/MoO_3 heterostructures and (b) out-plane Mo_2C/MoO_3 heterostructures.

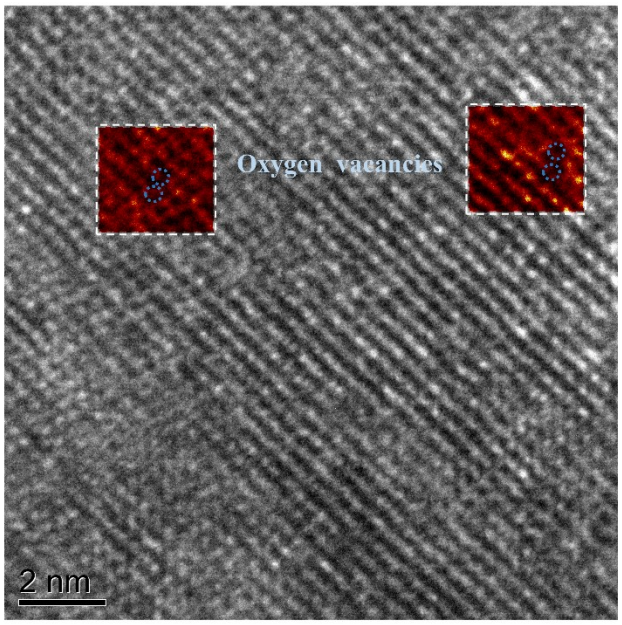

Figure S10. HRTEM images with oxygen vacancies were obtained.

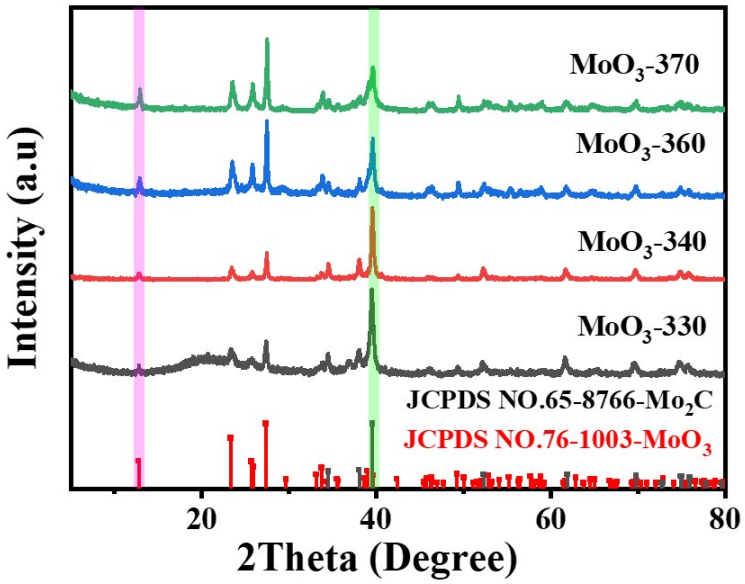

Figure S11. The XRD spectra of the samples were compared.

Table S1. Comparison of the TEA gas sensing performances with other semiconducting metal oxide materials.

Sensing material	TEA (ppm)	T/°C	Response (R_a/R_g)	LOD	Ref
Co_3O_4	100	160	31.27	50ppb	[3]
Co/Mo-Co_3O_4	100	160	126	300ppb	[4]
α-MoO_3	100	300	101.74	100ppb	[5]
Cr-MoO_3	100	200	150.27	\	[6]
MoO_3 microsheets	100	275	27.1	\	[7]
MoO_3	100	250	416	500ppb	[8]
SnO_2	100	270	49.2	1.01ppm	[9]
TiO_2/SnO_2	50	260	52.3	2ppm	[10]
Al_2O_3/α-Fe_2O_3	100	250	84.18	\	[11]
Pd-In_2O_3	50	220	47.56	1ppm	[12]
Mo_2C/MoO_3	**50**	**160**	**262.17**	**75 ppb**	**This work**

Reference:

1 J.P. Perdew, W. Yang, K. Burke, Z. Yang, E.K. Gross, M. Scheffler, G.E. Scuseria, T.M. Henderson, I.Y. Zhang, A. Ruzsinszky, H. Peng, J. Sun, E. Trushin, A. Gorling, Understanding band gaps of solids in generalized Kohn-Sham theory, Proc. Natl. Acad. Sci. U. S. A., 114 (2017) 2801-2806.

2 S. He, W. Li, L. Feng, W. Yang, Rational interaction between the aimed gas and oxide surfaces enabling high-performance sensor: The case of acidic α-MoO_3 nanorods for selective detection of triethylamine, J. Alloys. and Compd., 783 (2019) 574-582.

3 L. Du, H. Sun, Y. Liu, Metal-organic framework-derived hierarchical flower-like Mo-doped Co_3O_4 for enhanced triethylamine sensing properties, J. Alloys. Compd., 900 (2022) 163470.

4 H. Sun, X. Tang, S. Li, Y. Yao, L. Liu, MOF-derived one-dimensional Ru/Mo co-doped Co_3O_4 hollow microtubes for high-performance triethylamine sensing, Sensor Actuat B-Chem., 383 (2023) 133583.

5 K. He, S. He, W. Yang, Q. Tian, Ag nanoparticles-decorated α-MoO_3 nanorods for remarkable and rapid triethylamine-sensing response boosted by pulse-heating technique, J. Alloys. Compd., 808 (2019) 151704.

6 W. Li, S. He, L. Feng, W. Yang, Cr-doped α-MoO_3 nanorods for the fast detection of triethylamine using a pulse-heating strategy, Mater Lett., 250 (2019) 143-146.

7 W. Jiang, D. Wei, S. Zhang, X. Chuai, P. Sun, F. Liu, Y. Xu, Y. Gao, X. Liang, G. Lu, The facile synthesis of MoO_3microsheets and their excellent gas-sensing performance toward triethylamine: high selectivity, excellent stability and superior repeatability, New J. Chem., 42 (2018) 15111-15120.

8 L. Sun, G. Xie, P. Wu, Y. Xiong, L. Xu, Polarization effect of MoO_3 increases the thermoelectric properties based on the PbS quantum-dots doped P3HT Devices, ACS Appl. Polym., 1 (2019) 1054-1060.

9 Y. Zou, S. Chen, J. Sun, J. Liu, Y. Che, X. Liu, J. Zhang, D. Yang, Highly efficient gas sensor using a hollow SnO_2 microfiber for triethylamine detection, ACS Sens., 2 (2017) 897-902.

10 H. Xu, J. Ju, W. Li, J. Zhang, J. Wang, B. Cao, Superior triethylamine-sensing properties based on TiO_2/SnO_2 n–n heterojunction nanosheets directly grown on ceramic tubes, Sensor Actuat B-Chem., 228 (2016) 634-642.

11 L. Guo, C. Wang, X. Kou, N. Xie, F. Liu, H. Zhang, X. Liang, Y. Gao, Y. Sun, X. Chuai, G. Lu, Detection of triethylamine with fast response by Al_2O_3/α-Fe_2O_3 composite nanofibers, Sensor Actuat B-Chem., 266 (2018) 139-148.

12 X. Liu, K. Zhao, X. Sun, C. Zhang, X. Duan, P. Hou, G. Zhao, S. Zhang, H. Yang, R. Cao, X. Xu, Rational design of sensitivity enhanced and stability improved TEA gas sensor assembled with Pd nanoparticles-functionalized In_2O_3 composites, Sensor Actuat B-Chem., 285 (2019) 1-10.